Supplement of

Implementing the Nitrogen cycle into the dynamic global vegetation, hydrology and crop growth model LPJmL

W. von Bloh et al.

Correspondence to: Werner von Bloh (bloh@pik-potsdam.de)

S1 Supplementary information to the nitrogen implementation of the LPJmL5 model

The supplement contains tables of parameters used in the model (Table S1 and S2) and graphical representations of leaf C:N ratios for different exponential factors (Fig. S1), daily gross photosynthesis rate as a function of light- and Rubisco limited photosynthesis rate (Fig. S2), temperature response function $F_1(T)$ (Fig. S3), and water response function $F_2(W)$ (Fig. S4). Furthermore comparisons of net ecosystem exchange rates and evaporation fluxes with EDDY flux tower measurements (ORNL DAAC, 2011) for a variety of sites are shown (Figs. S5-S11 and Figs. S12-S20, respectively). Taylor diagrams of the spatial patterns (national mean yields) of wheat, maize, rice and soybean are plotted in Figs. S21-S24. Wheat, rice and soybean simulations for the 10 top-producing countries for the carbon-only LPJmL3.5 version, the version with N limitation and with unlimited N supply are shown in Figs. S25-S27.

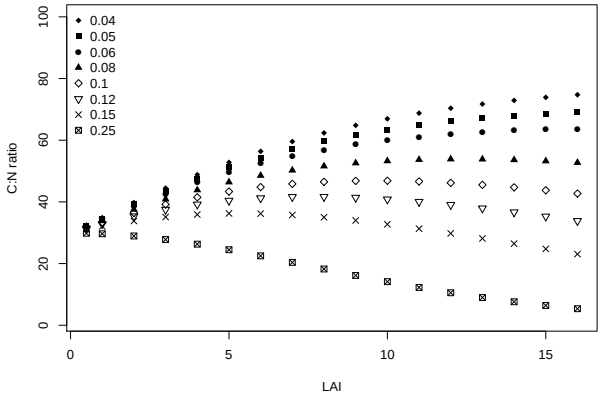

Figure S1. Leaf C:N ratio of the canopy as a function of LAI for different pre-factors of the exponential term in Eq. (2).

Table S1. List of PFT-specific parameters (maximum N uptake rate $N_{\mathrm{up,root}}$, increase in N demand k_{store}, N recover fraction at turnover k_{turn}, minimum canopy conductance g_{min}, maximum water transport capacity E_{max}) used in the LPJmL5 model.

PFT	$N_{\mathrm{up,root}}$ (gN kgC^{-1})	k_{store}	k_{turn} (%)	g_{min} (mm s^{-1})	E_{max} (mm day^{-1})
Tropical broadleaved evergreen tree	2.8	1.15	80	1.6	10
Tropical broadleaved raingreen tree	2.8	1.15	30	1.8	10
Temperate needleleaved evergreen tree	2.8	1.15	80	1.0	7
Temperate broadleaved evergreen tree	2.8	1.15	80	1.5	7
Temperate broadleaved summergreen tree	2.8	1.15	30	1.0	7
Boreal needleleaved evergreen tree	2.8	1.15	80	0.8	7
Boreal broadleaved summergreen tree	2.8	1.15	30	0.8	7
Boreal needleleaved summergreen tree	2.8	1.15	30	0.3	7
C3 perennial grass	5.1	1.3	30	0.8	7
C4 perennial grass	5.1	1.3	30	1.5	10
All crops	5.1	1.3	30	0.8	8

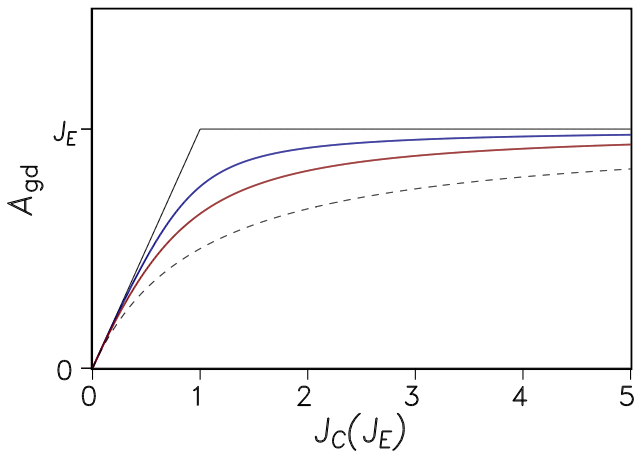

Figure S2. Daily gross photosynthesis rate A_{gd} as a function of Rubisco-limited photosynthesis rate J_C for fixed light-limited rate J_E and daylength set to 1. The black solid curve is for shape parameter $\theta = 1$ ($A_{\mathrm{gd}} = \min(J_E, J_C)/\mathrm{daylength}$), the blue curve for $\theta = 0.9$ (LPJmL5), the red curve for $\theta = 0.7$ (LPJmL3.5) and the black dashed curve for $\theta \to 0$ ($A_{\mathrm{gd}} = J_E \cdot J_C/((J_E + J_C) \cdot \mathrm{daylength})$).

Table S2. List of parameters used in the LPJmL5 model.

Parameter	Description	Value	Units
α_a	Fraction of PAR assimilated at ecosystem level, relative to leaf level	0.6	-
α_m	Maximum Priestley-Taylor coefficient	1.485	-
g_m	Conductance scaling factor	2.41	-
θ	Shape parameter for co-limitation of photosynthesis	0.9	-
$K_{\mathrm{N,min}}$	Michaelis constant of N uptake	1.48	gN m^{-2}
$k_{\mathrm{N,min}}$	Basal rate of N uptake	0.05	-
$f_{\mathrm{heartwood}}$	Fraction of sapwood nitrogen going into heartwood	0.7	-
K_M	Michaelis constant of photosynthesis reduction	0.1	-
$K_{\max}$	Maximum rate of NH_4^+ nitrified	0.1	d^{-1}
a	Parameter in limiting function for temperature $F_1(T)$	8.79	°C
b	Parameter in limiting function for temperature $F_1(T)$	5.26	-
a_{nit}	Parameter in water response function $F_1(W_{\mathrm{sat}})$	0.6 (medium soil), 0.55 (sandy soil)	-
b_{nit}	Parameter in water response function $F_1(W_{\mathrm{sat}})$	1.27 (medium soil), 1.7 (sandy soil)	-
c_{nit}	Parameter in water response function $F_1(W_{\mathrm{sat}})$	0.001 (medium soil), -0.007 (sandy soil)	-
d_{nit}	Parameter in water response function $F_1(W_{\mathrm{sat}})$	2.84 (medium soil), 3.22 (sandy soil)	-
CDN	Shape coefficient for $F_2(T, C)$	1.4	-
A_f	Fraction of decomposed N mineralized	0.6	-
F_f	Fraction of humified N going into fast pool	0.98	-
$\beta_{\mathrm{NO}_3^-}$	NO_3^- percolation coefficient	0.4	-
$\mathrm{CN}_{\mathrm{soil}}$	Desired C:N ratio of soils	15	-
k^f_{soil10}	Decomposition rate of fast pool	0.03	yr^{-1}
k^s_{soil10}	Decomposition rate of slow pool	0.001	yr^{-1}
r_{mx}	Fraction of denitrified N lost as $\mathrm{N_2O}$	0.11	-
θ	Fractional pore space	0.4	-
K_2	Fraction of nitrified N lost as $\mathrm{N_2O}$ flux	0.02	-
K_N	Michaelis constant of N immobilization	5×10^{-3}	gN m^{-3}
T_0	Parameter in temperature uptake function	-25	°C
T_m	Parameter in temperature uptake function	15	°C
T_r	Parameter in temperature uptake function	15	°C
q_{ash}	Fraction of fire N going to the top soil layer	0.45	-

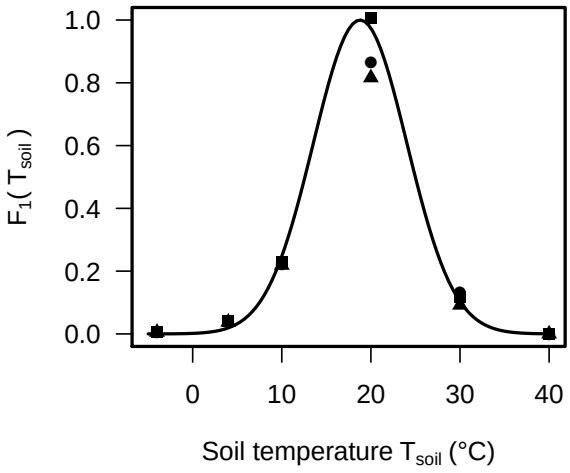

Figure S3. Temperature response data for site in the US (filled squares), Canada (filled circles) and Australia (filled triangles) and fitted function (solid line) used in Eq. (36).

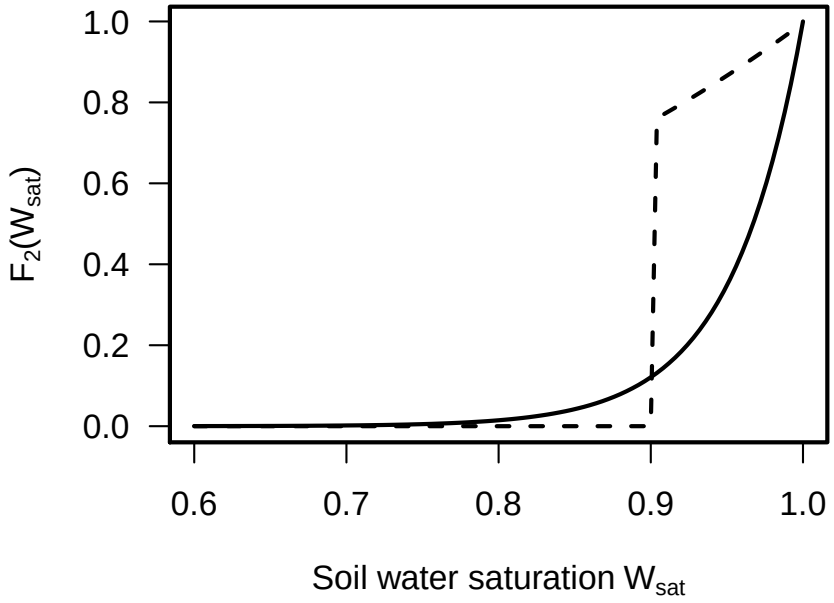

Figure S4. Water response functions $F_2(W_{\mathrm{sat}})$ parameterized according to Krysanova and Wechsung (2000) (dashed line) and according to Eq. (43) in the main text (solid line).

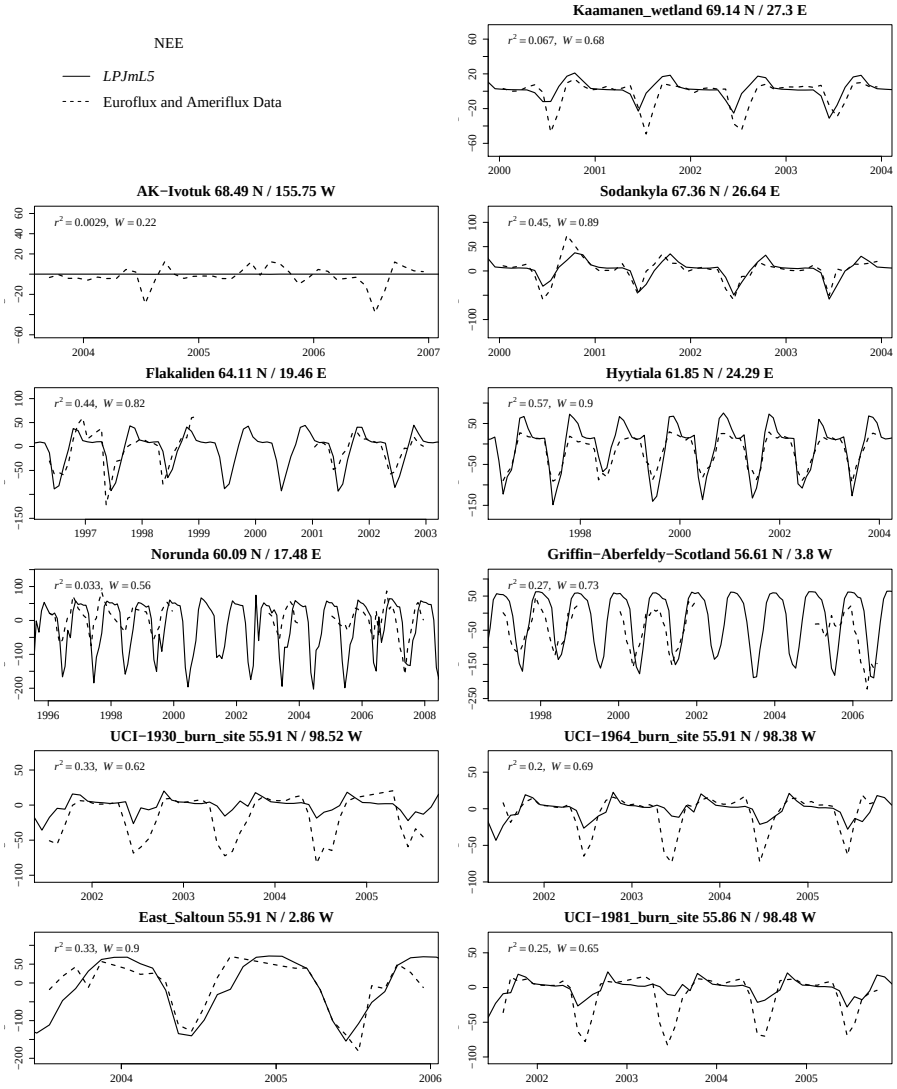

Figure S5. Comparison of net ecosystem exchange rates (NEE, in gC m^{-2} d^{-1}) simulated with eddy flux tower rates measured, W denotes the Willmott coefficient of agreement.

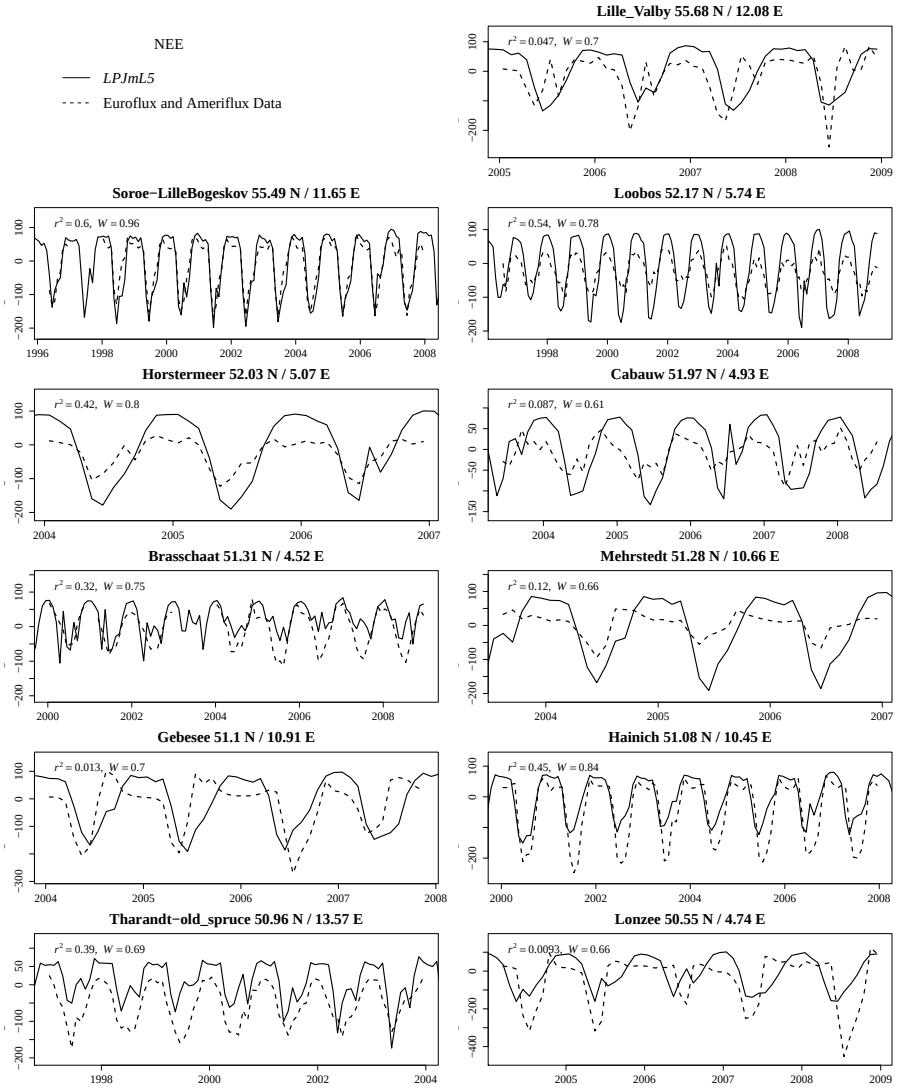

Figure S6. Comparison of net ecosystem exchange rates (NEE, in gC m^{-2} d^{-1}) simulated with eddy flux tower rates measured, W denotes the Willmott coefficient of agreement.

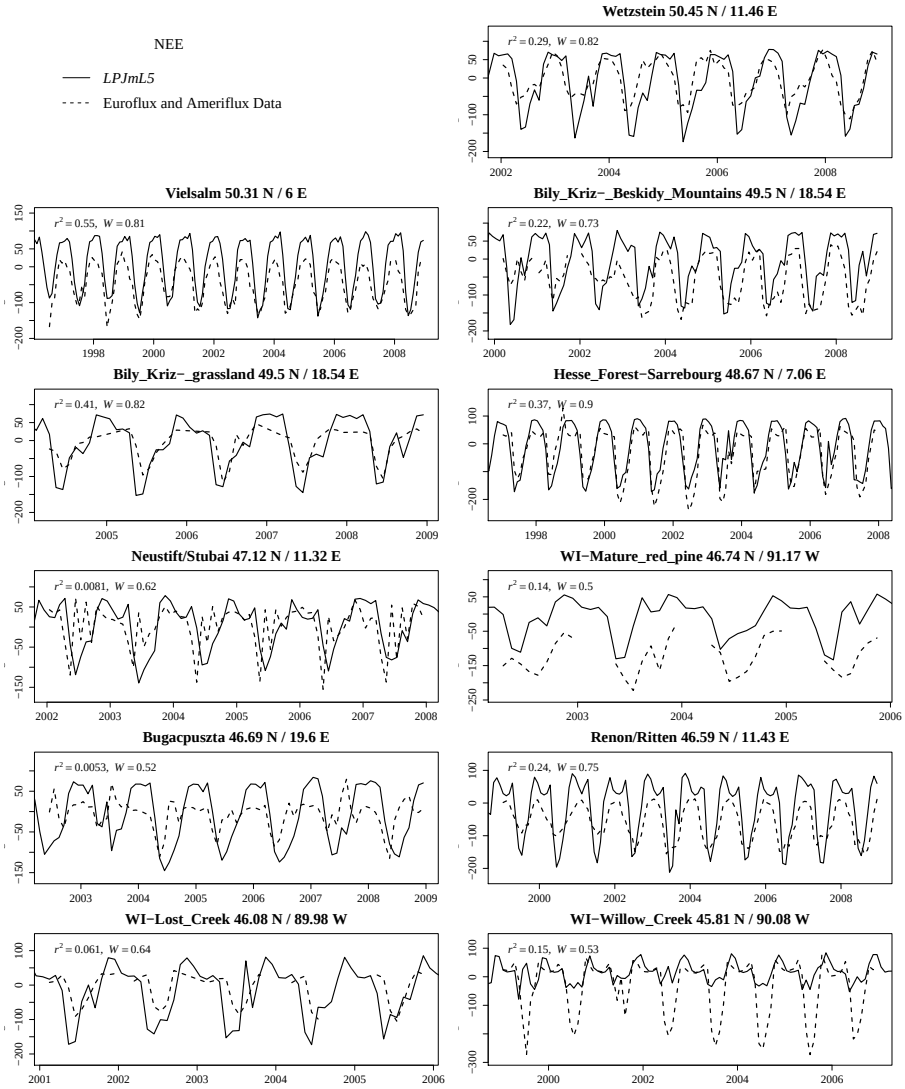

Figure S7. Comparison of net ecosystem exchange rates (NEE, in gC m^{-2} d^{-1}) simulated with eddy flux tower rates measured, W denotes the Willmott coefficient of agreement.

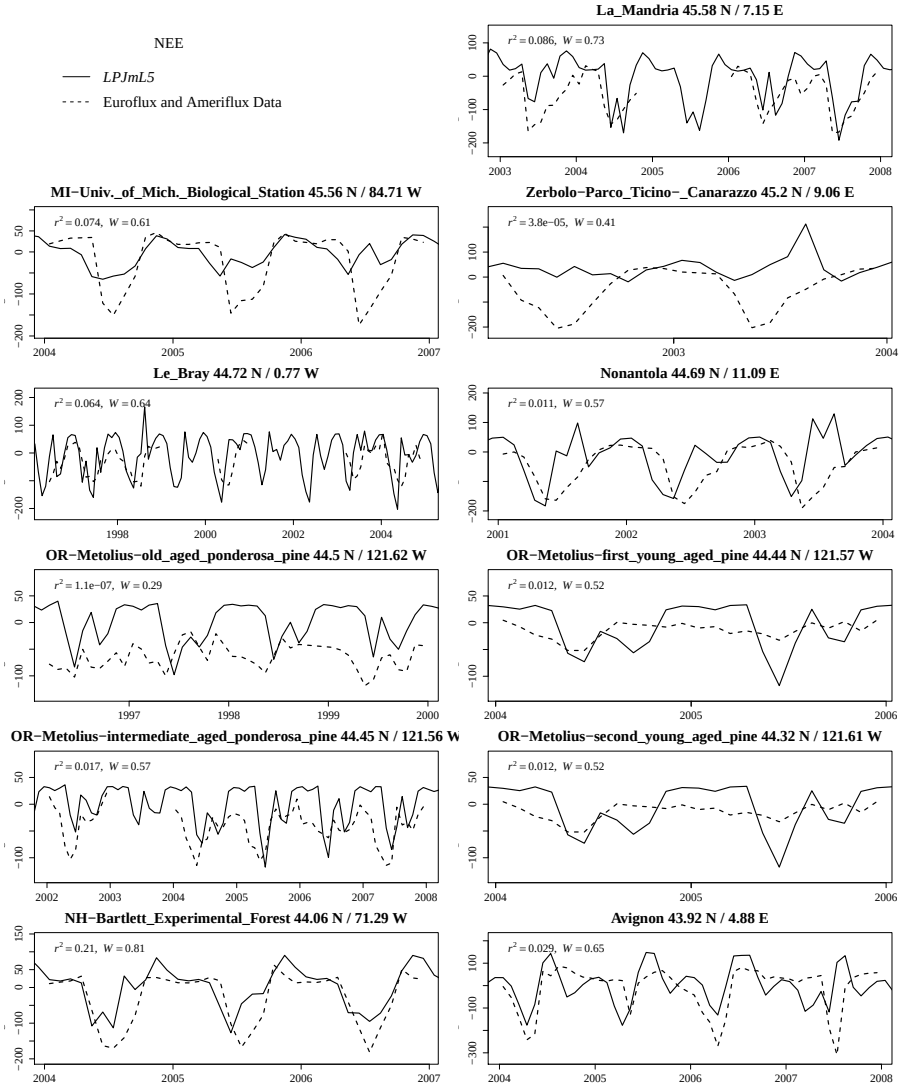

Figure S8. Comparison of net ecosystem exchange rates (NEE, in gC m^{-2} d^{-1}) simulated with eddy flux tower rates measured, W denotes the Willmott coefficient of agreement.

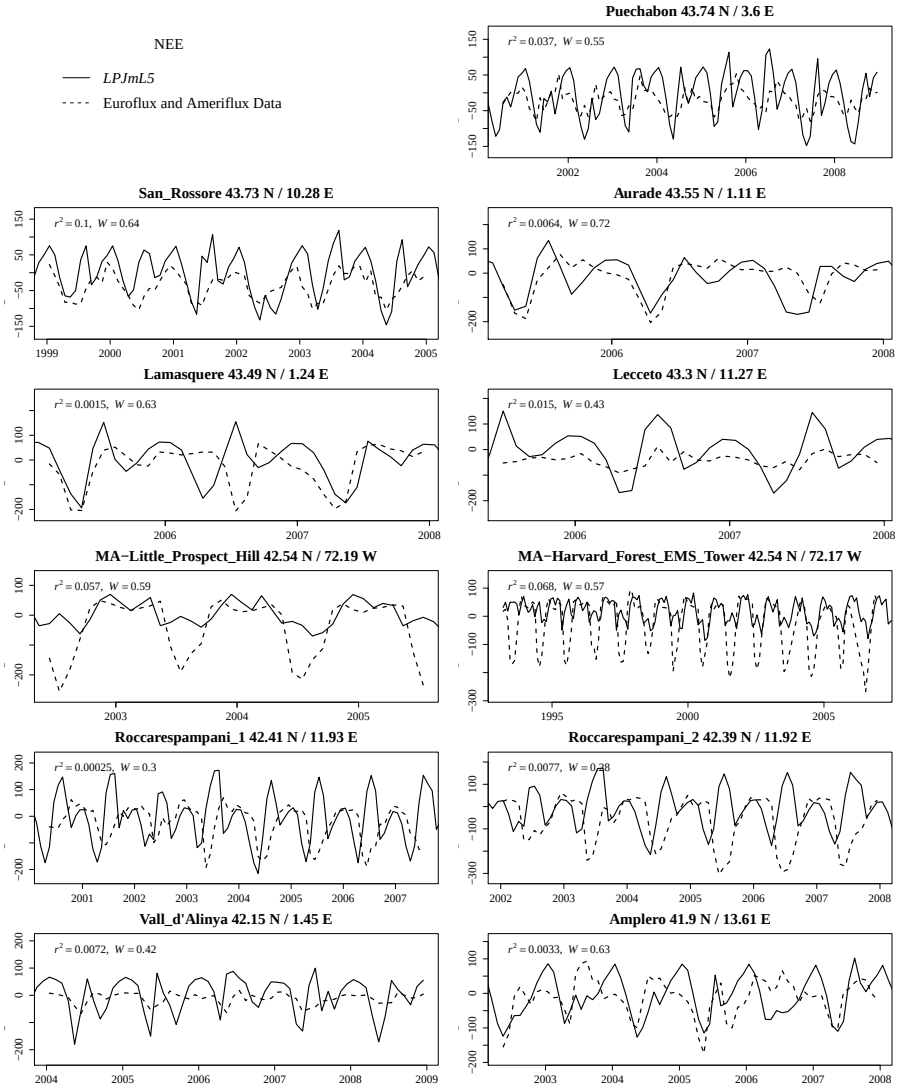

Figure S9. Comparison of net ecosystem exchange rates (NEE, in gC m^{-2} d^{-1}) simulated with eddy flux tower rates measured, W denotes the Willmott coefficient of agreement.

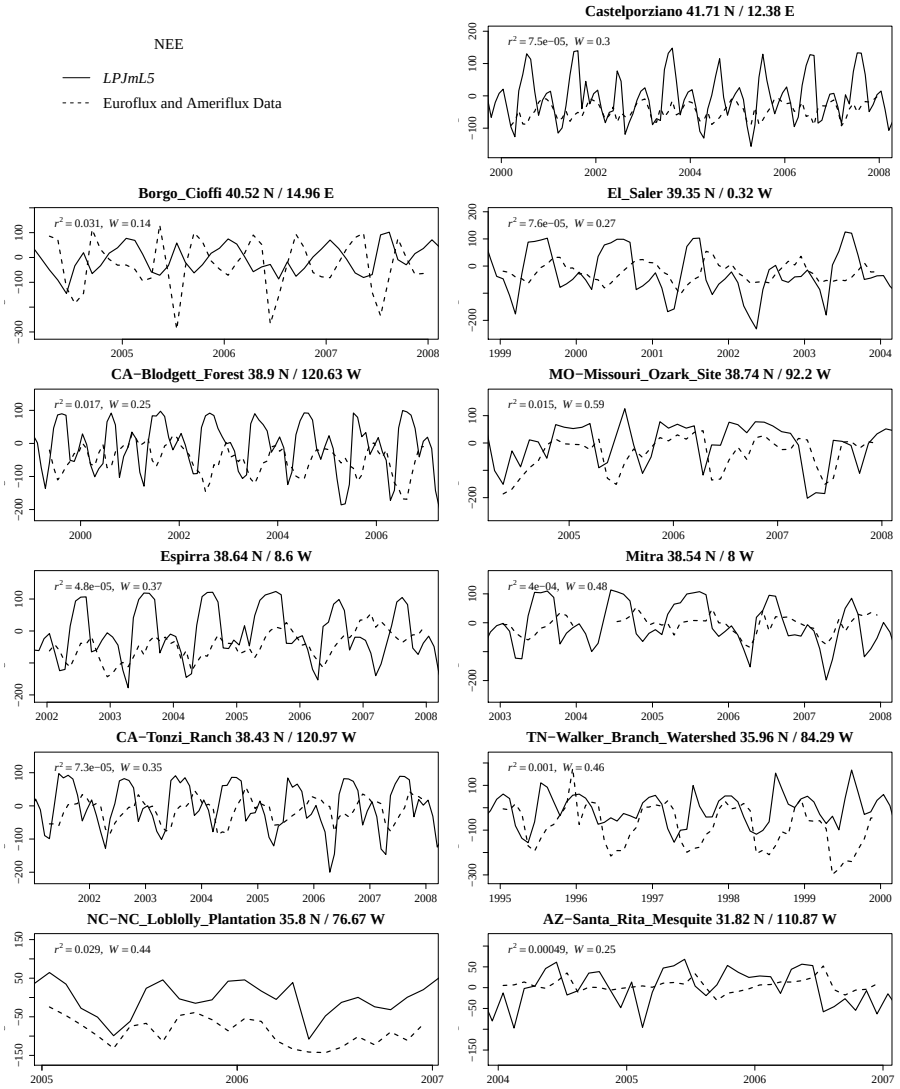

Figure S10. Comparison of net ecosystem exchange rates (NEE, in gC m^{-2} d^{-1}) simulated with eddy flux tower rates measured, W denotes the Willmott coefficient of agreement.

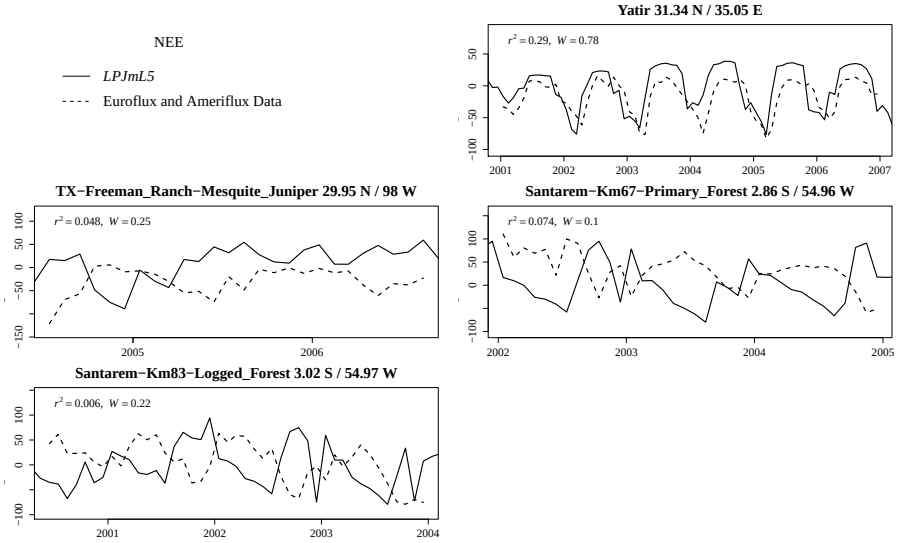

Figure S11. Comparison of net ecosystem exchange rates (NEE, in gC m^{-2} d^{-1}) simulated with eddy flux tower rates measured.

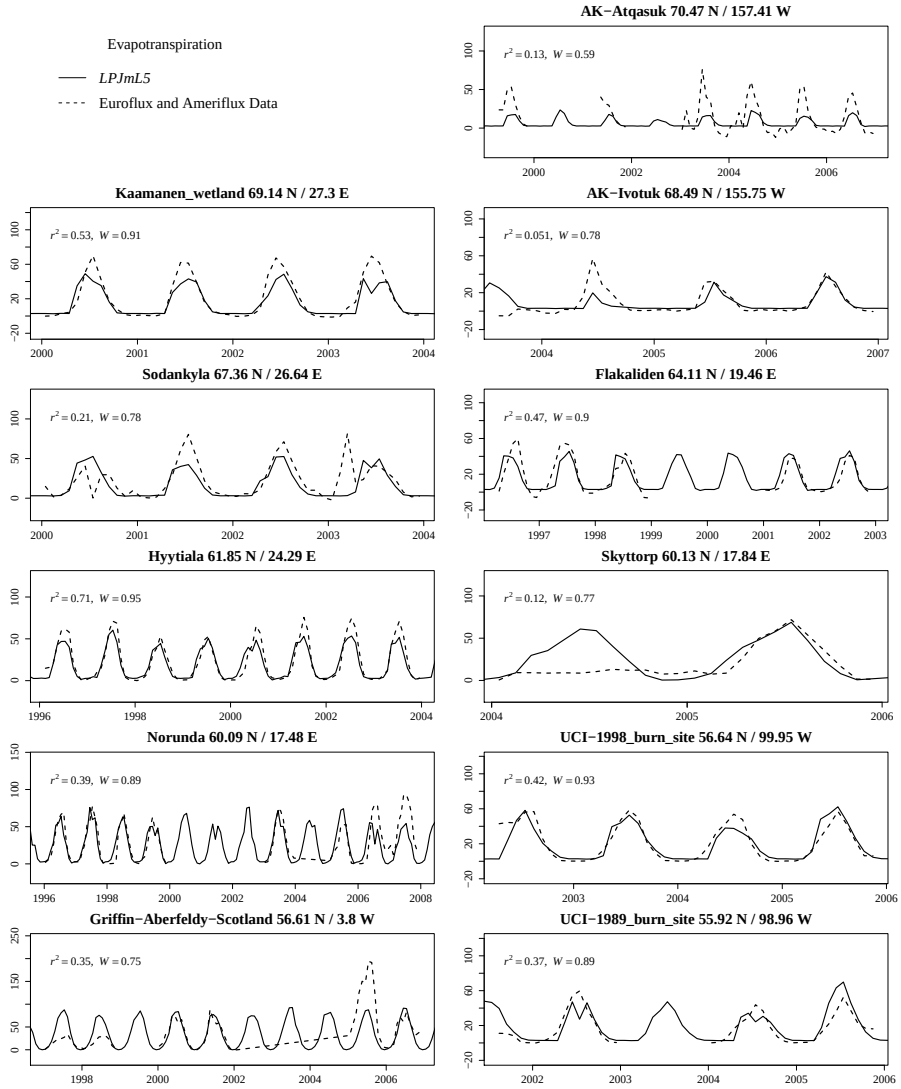

Figure S12. Comparison of evapotranspiration fluxes (in mm d^{-1}) with EDDY-flux measurements, W denotes the Willmott coefficient of agreement.

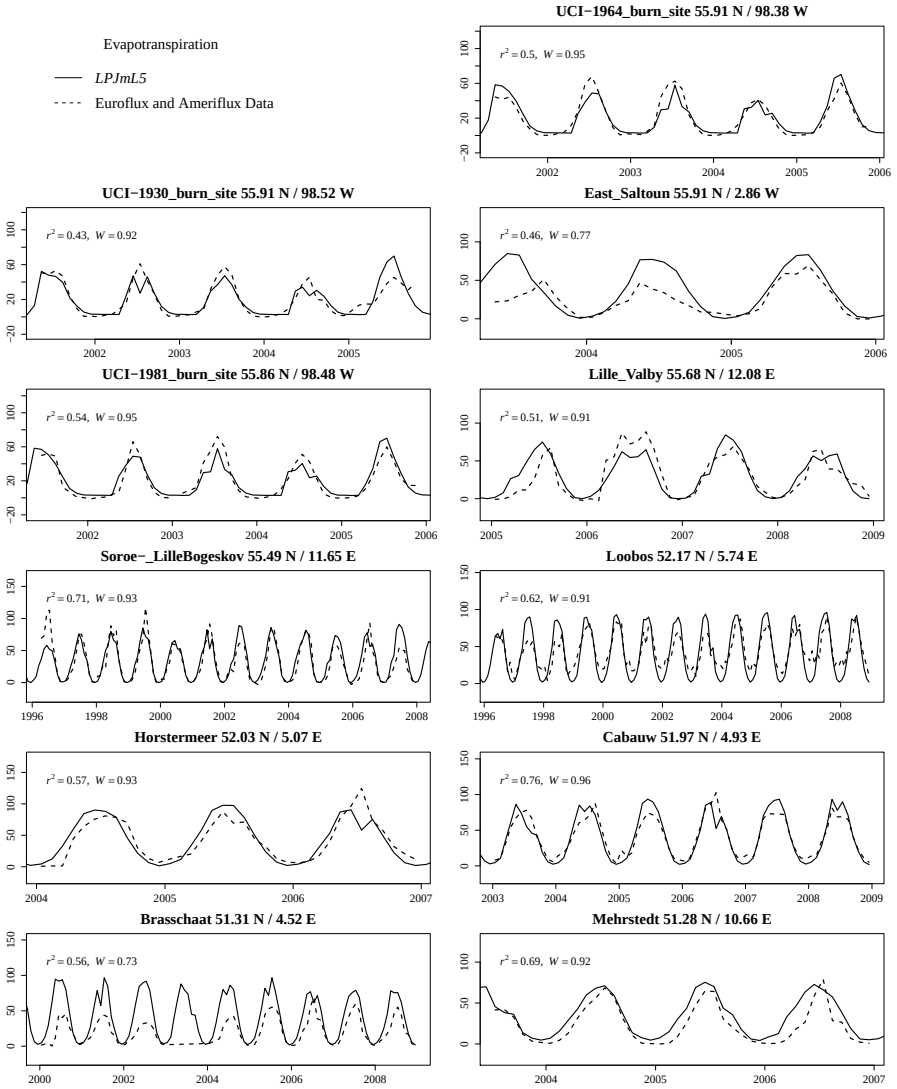

Figure S13. Comparison of evapotranspiration fluxes (in mm d^{-1}) with EDDY-flux measurements, W denotes the Willmott coefficient of agreement.

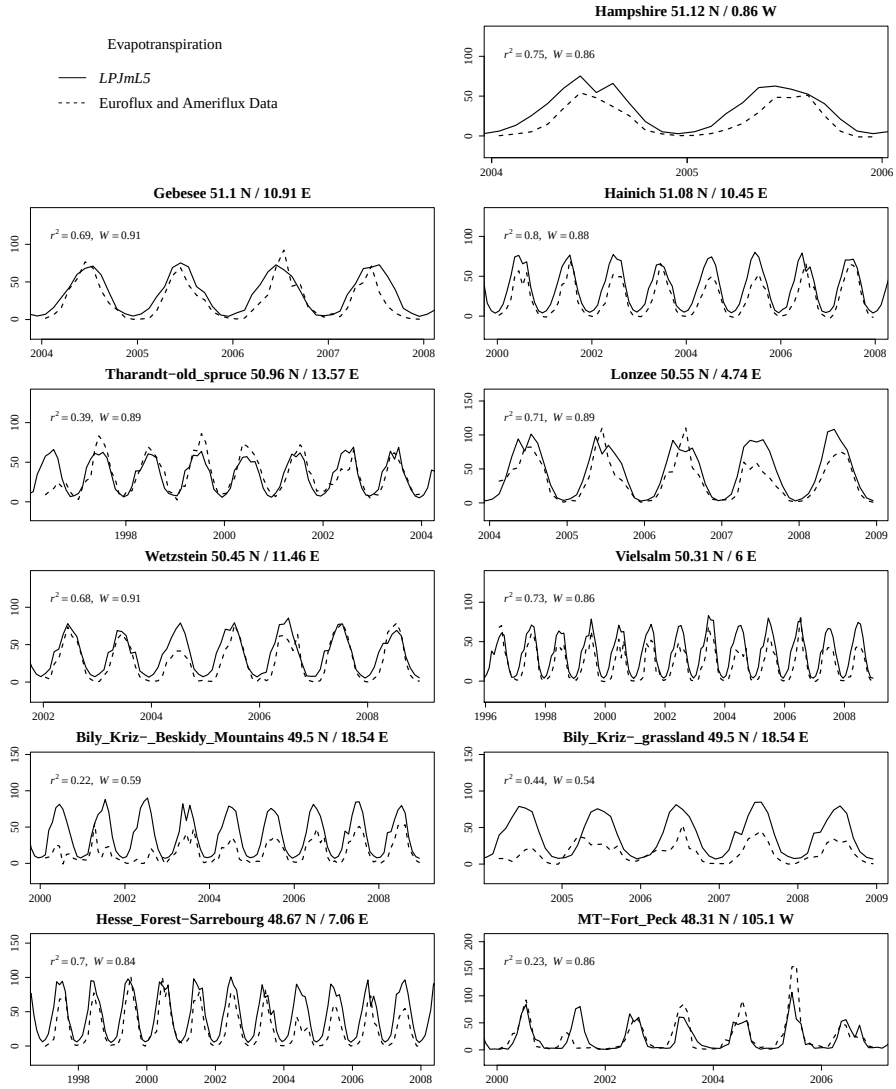

Figure S14. Comparison of evapotranspiration fluxes (in mm d^{-1}) with EDDY-flux measurements, W denotes the Willmott coefficient of agreement.

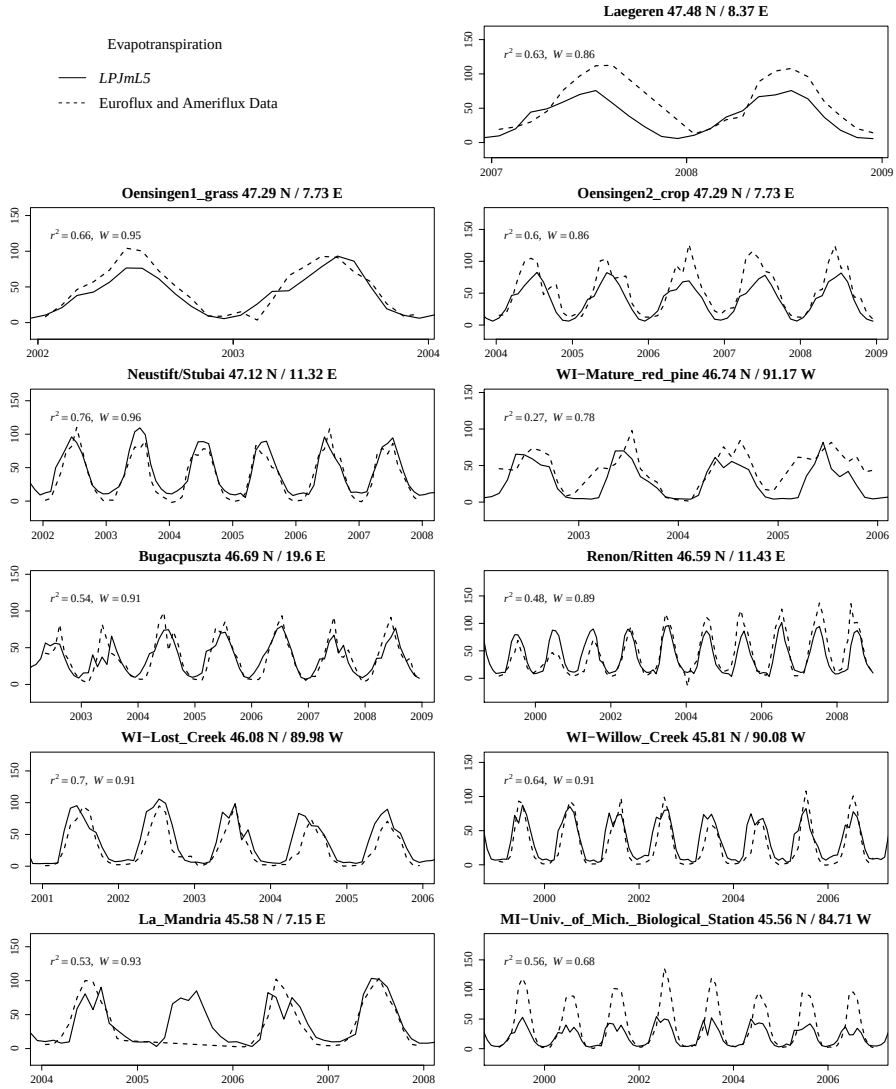

Figure S15. Comparison of evapotranspiration fluxes (in mm d^{-1}) with EDDY-flux measurements, W denotes the Willmott coefficient of agreement.

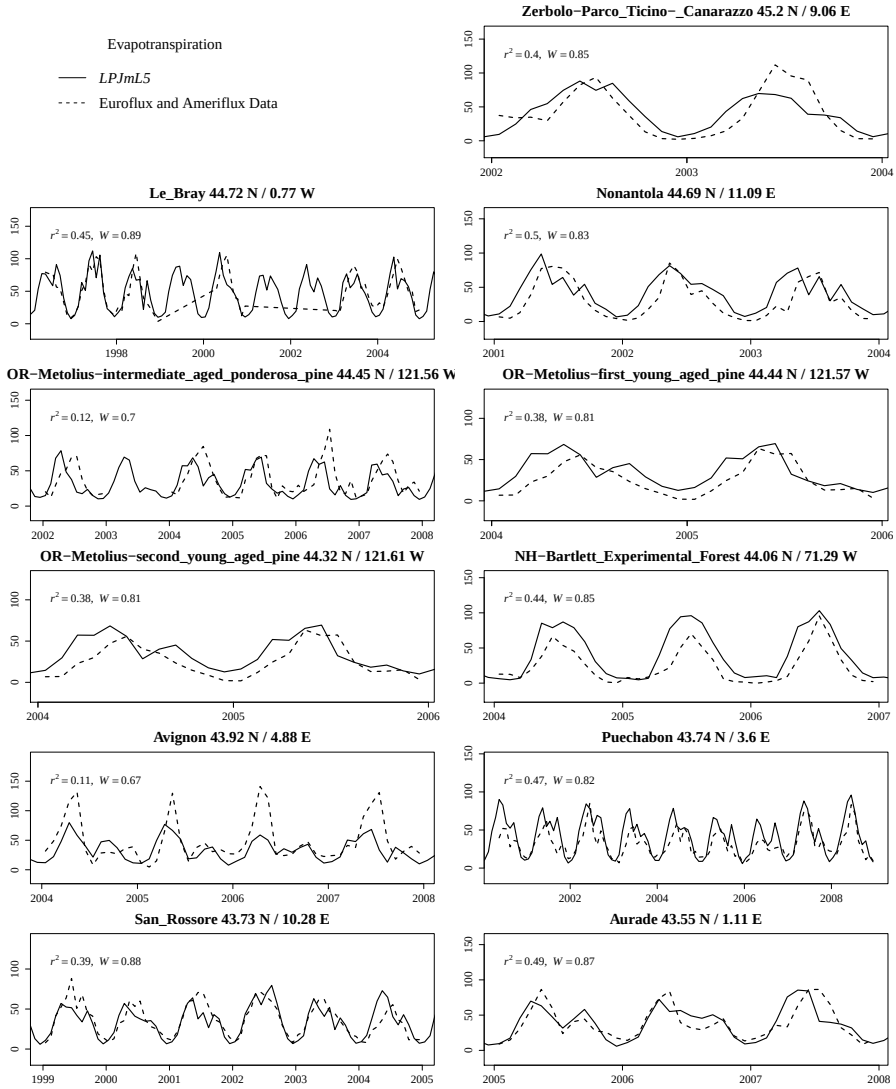

Figure S16. Comparison of evapotranspiration fluxes (in mm d^{-1}) with EDDY-flux measurements, W denotes the Willmott coefficient of agreement.

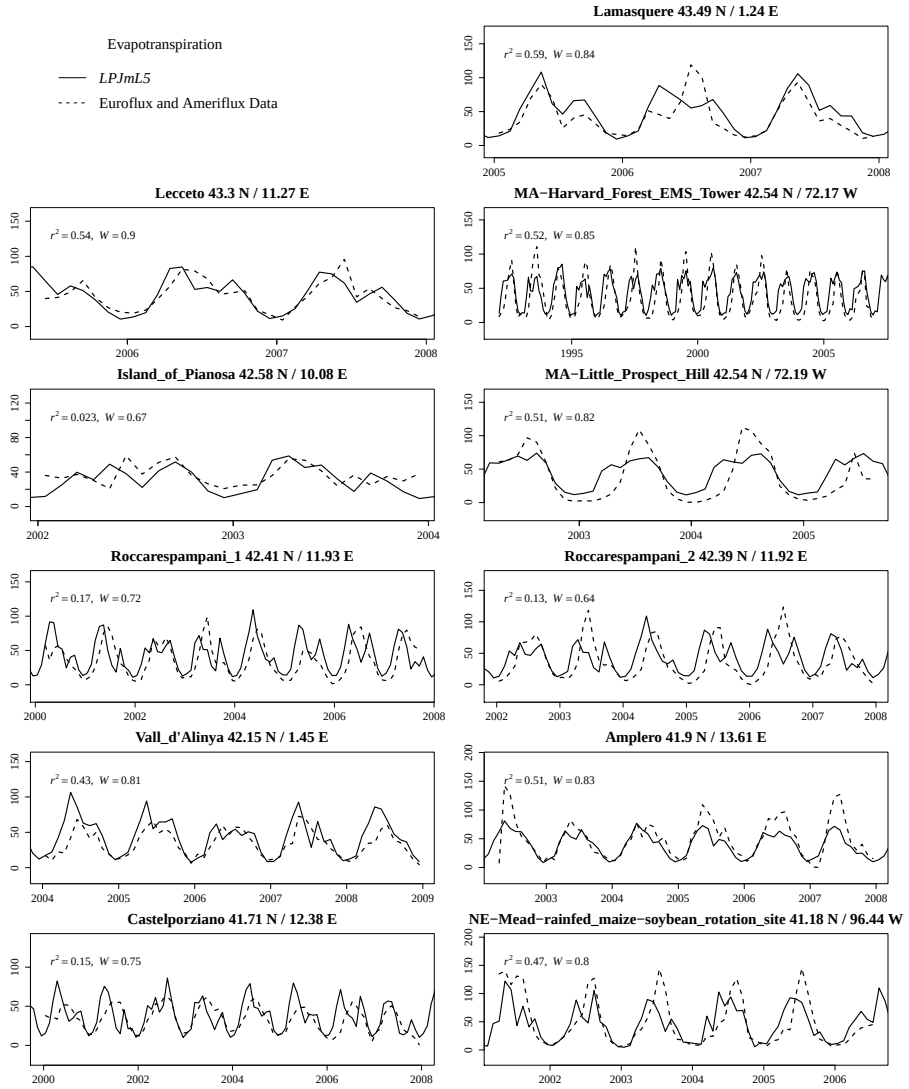

Figure S17. Comparison of evapotranspiration fluxes (in mm d^{-1}) with EDDY-flux measurements, W denotes the Willmott coefficient of agreement.

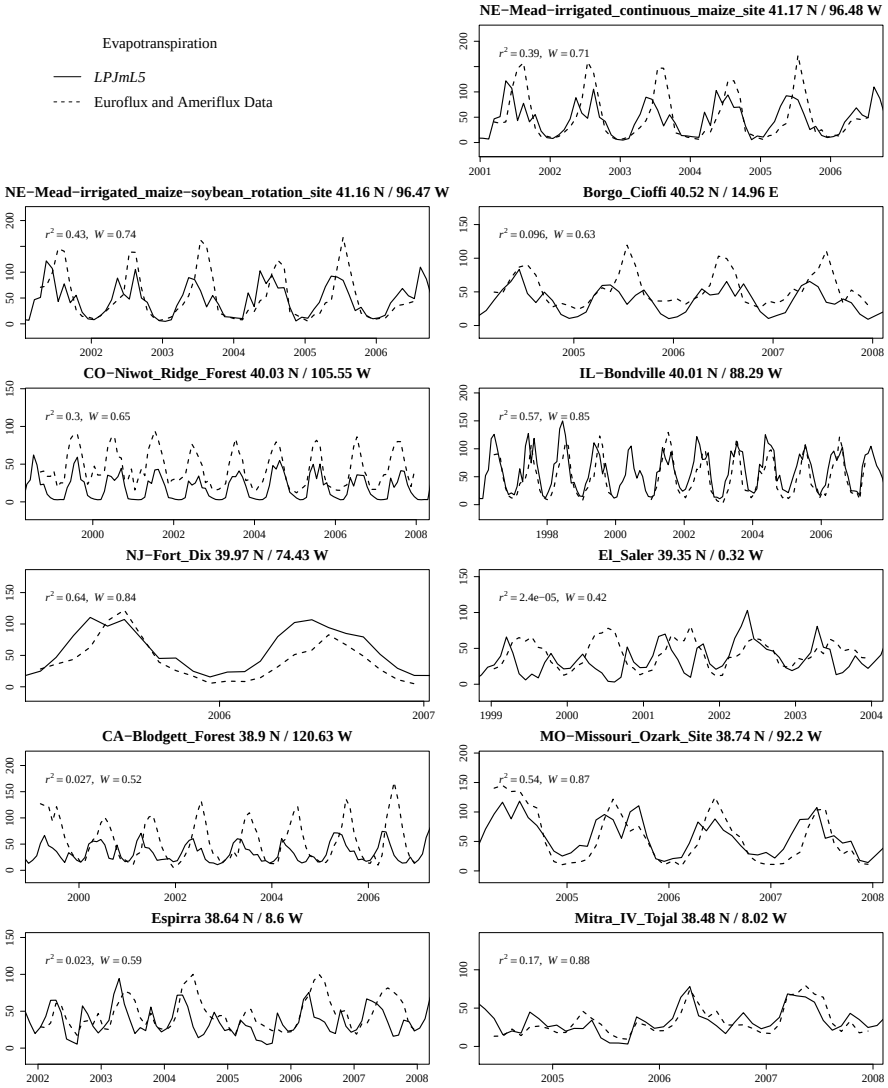

Figure S18. Comparison of evapotranspiration fluxes (in mm d^{-1}) with EDDY-flux measurements, W denotes the Willmott coefficient of agreement.

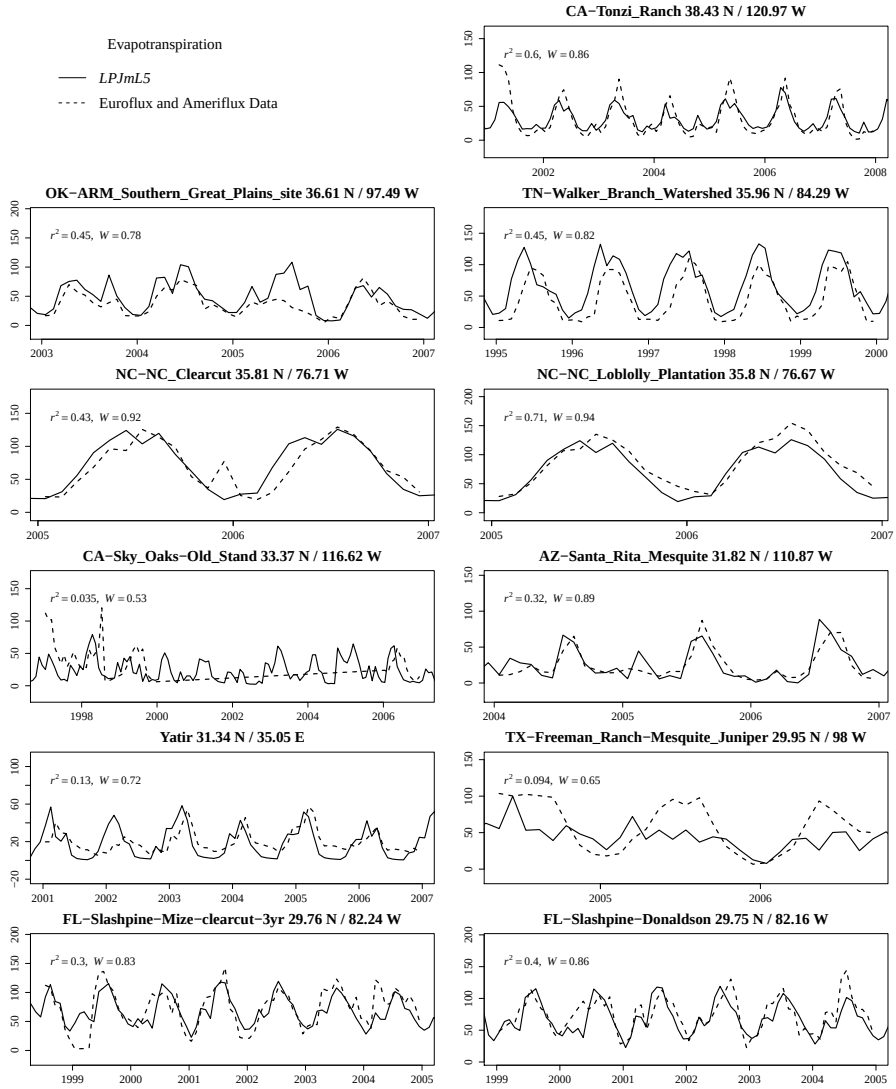

Figure S19. Comparison of evapotranspiration fluxes (in mm d^{-1}) with EDDY-flux measurements, W denotes the Willmott coefficient of agreement.

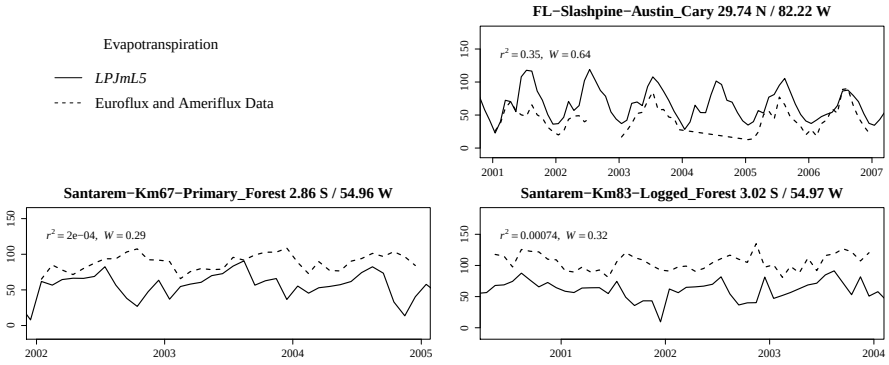

Figure S20. Comparison of evapotranspiration fluxes (in mm d^{-1}) with EDDY-flux measurements, W denotes the Willmott coefficient of agreement.

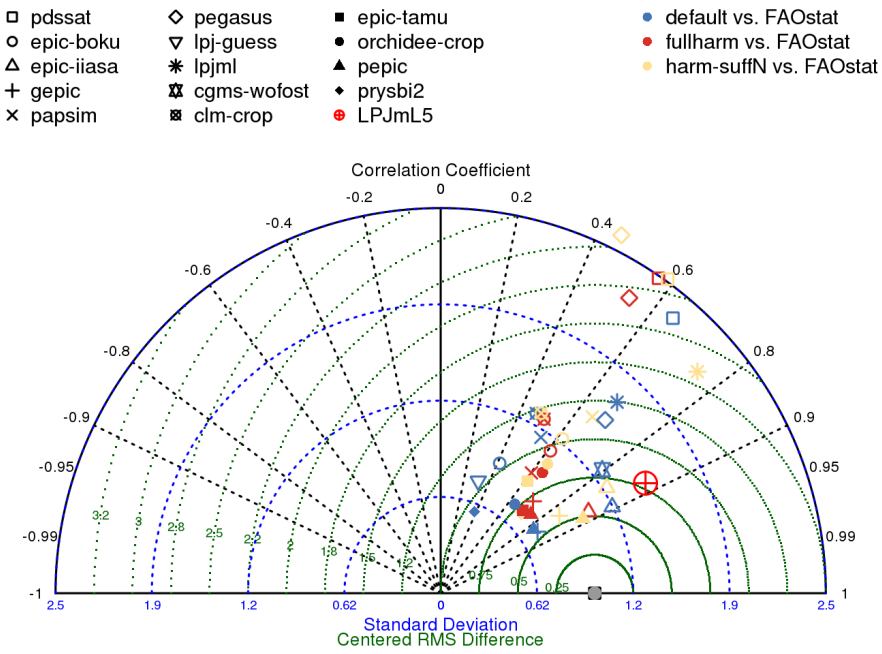

Figure S21. Taylor diagram of the spatial patterns (national mean yields) of wheat productivity. The performance of *LPJmL5* is depicted as the red circlecross (⊕) and should be compared to the *LPJmL3.5* simulations, depicted as stars (✳) in yellow (un-calibrated) and blue (calibrated). This figure was produced by the online crop model evaluation tool of Müller et al. (2017).

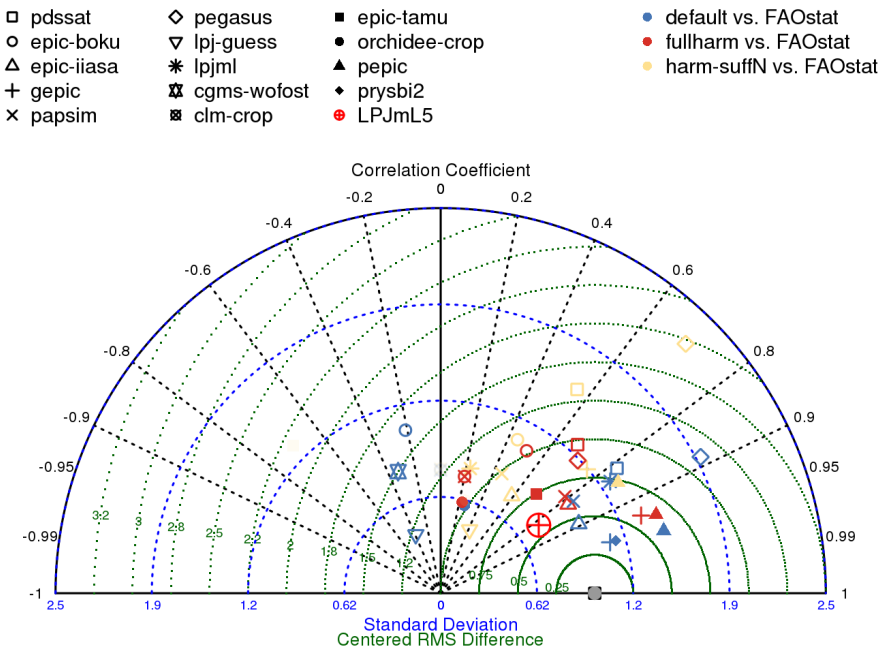

Figure S22. Taylor diagram of the spatial patterns (national mean yields) of maize productivity. The performance of *LPJmL5* is depicted as the red circlecross (⊕) and should be compared to the *LPJmL3.5* simulations, depicted as stars (✳) in yellow (uncalibrated) and blue (calibrated). This figure was produced by the online crop model evaluation tool of Müller et al. (2017).

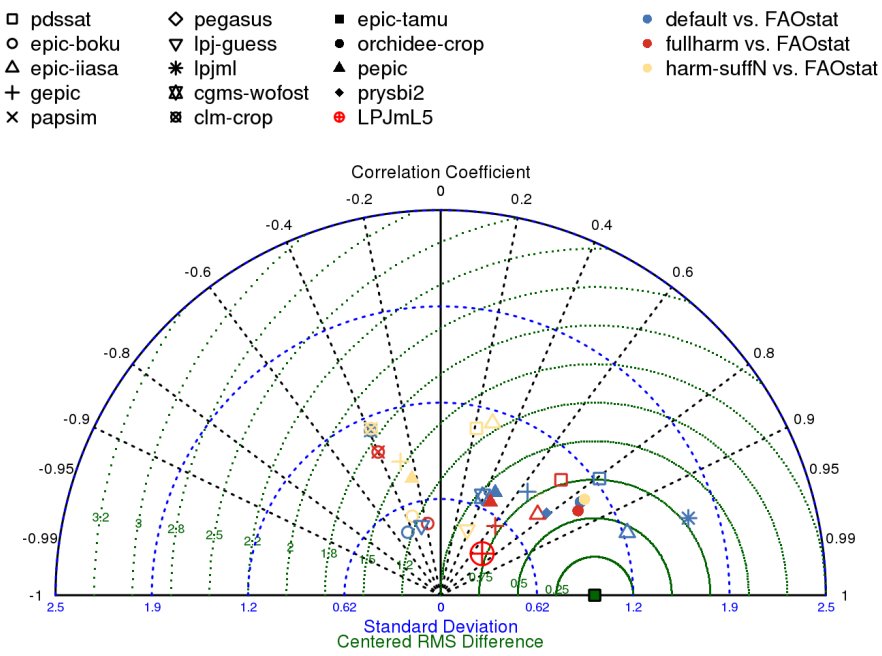

Figure S23. Taylor diagram of the spatial patterns (national mean yields) of rice productivity. The performance of *LPJmL5* is depicted as the red circlecross (⊕) and should be compared to the *LPJmL3.5* simulations, depicted as stars (✳) in yellow (un-calibrated) and blue (calibrated). This figure was produced by the online crop model evaluation tool of Müller et al. (2017).

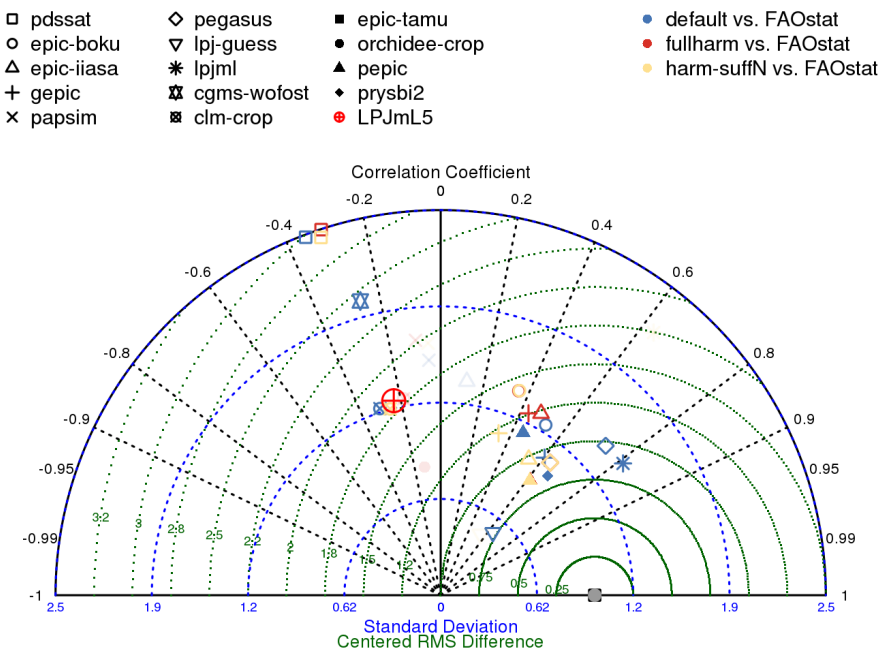

Figure S24. Taylor diagram of the spatial patterns (national mean yields) of soybean productivity. The performance of *LPJmL5* is depicted as the red circlecross (⊕) and should be compared to the *LPJmL3.5* simulations, depicted as stars (✳) in yellow (un-calibrated) and blue (calibrated). This figure was produced by the online crop model evaluation tool of Müller et al. (2017).

References

Krysanova, V. and Wechsung, F.: SWIM (Soil and Water Integrated Model) User Manual, https://www.pik-potsdam.de/members/valen/swim, 2000.

Müller, C., Elliott, J., Chryssanthacopoulos, J., Arneth, A., Balkovic, J., Ciais, P., Deryng, D., Folberth, C., Glotter, M., Hoek, S., Iizumi, T., Izaurralde, R. C., Jones, C., Khabarov, N., Lawrence, P., Liu, W., Olin, S., Pugh, T. A. M., Ray, D. K., Reddy, A., Rosenzweig, C., Ruane, A. C., Sakurai, G., Schmid, E., Skalsky, R., Song, C. X., Wang, X., de Wit, A., and Yang, H.: Global gridded crop model evaluation: benchmarking, skills, deficiencies and implications, Geoscientific Model Development, 10, 1403–1422, doi:10.5194/gmd-10-1403-2017, 2017.

ORNL DAAC, Oak Ridge, T. U.: Oak Ridge National Laboratory Distributed Active Archive Center (ORNL DAAC), http://fluxnet.ornl.gov/, 2011.

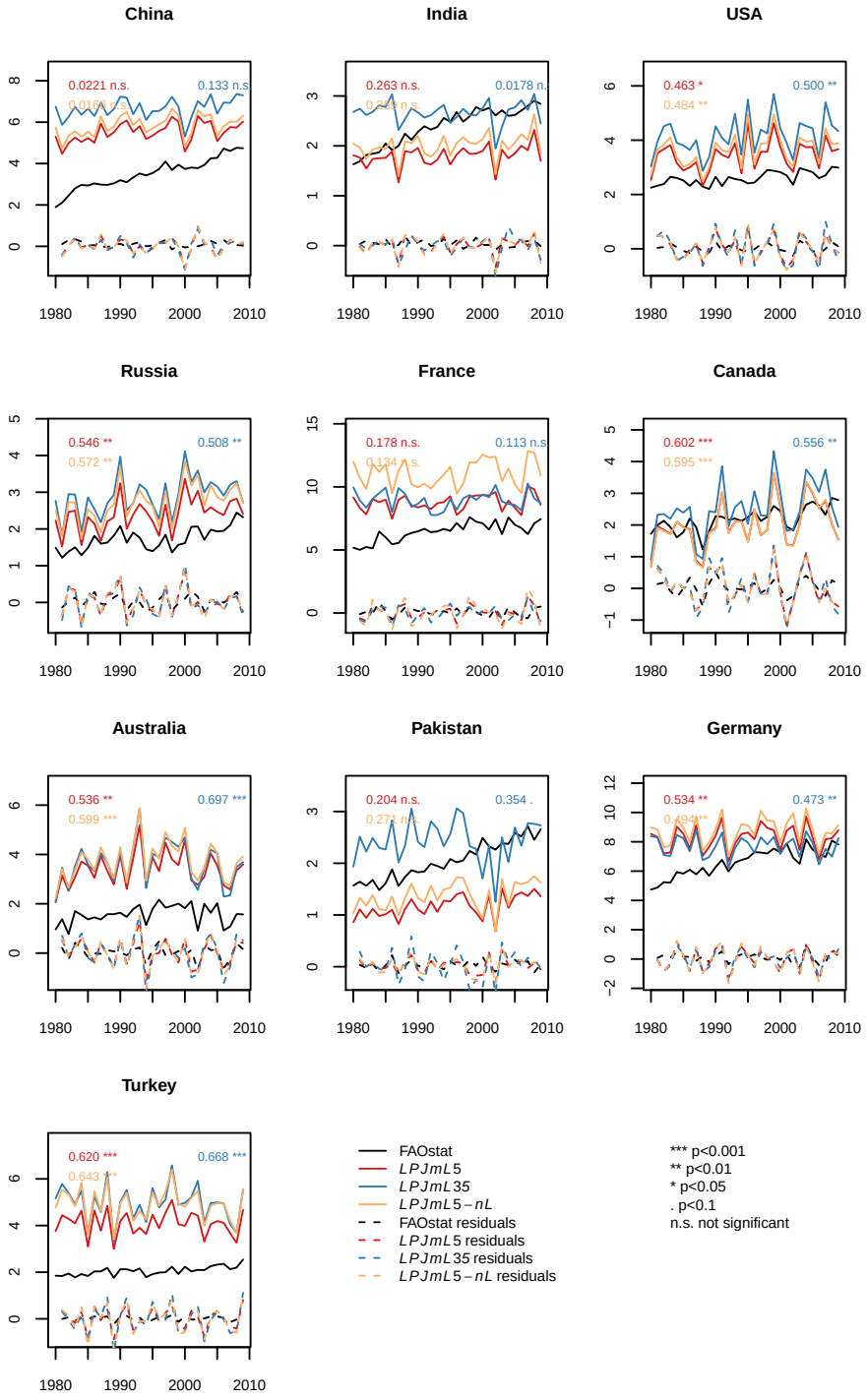

Figure S25. Wheat yield simulations (in t fresh matter (FM) ha^{-1}) for the 10 top-producing countries for the carbon-only LPJmL3.5 version (*LPJmL35*), the version with N limitation (*LPJmL5*)and with unlimited N supply (*LPJmL5-nL*). The residuals plotted are the detrended observed and simulated yields.

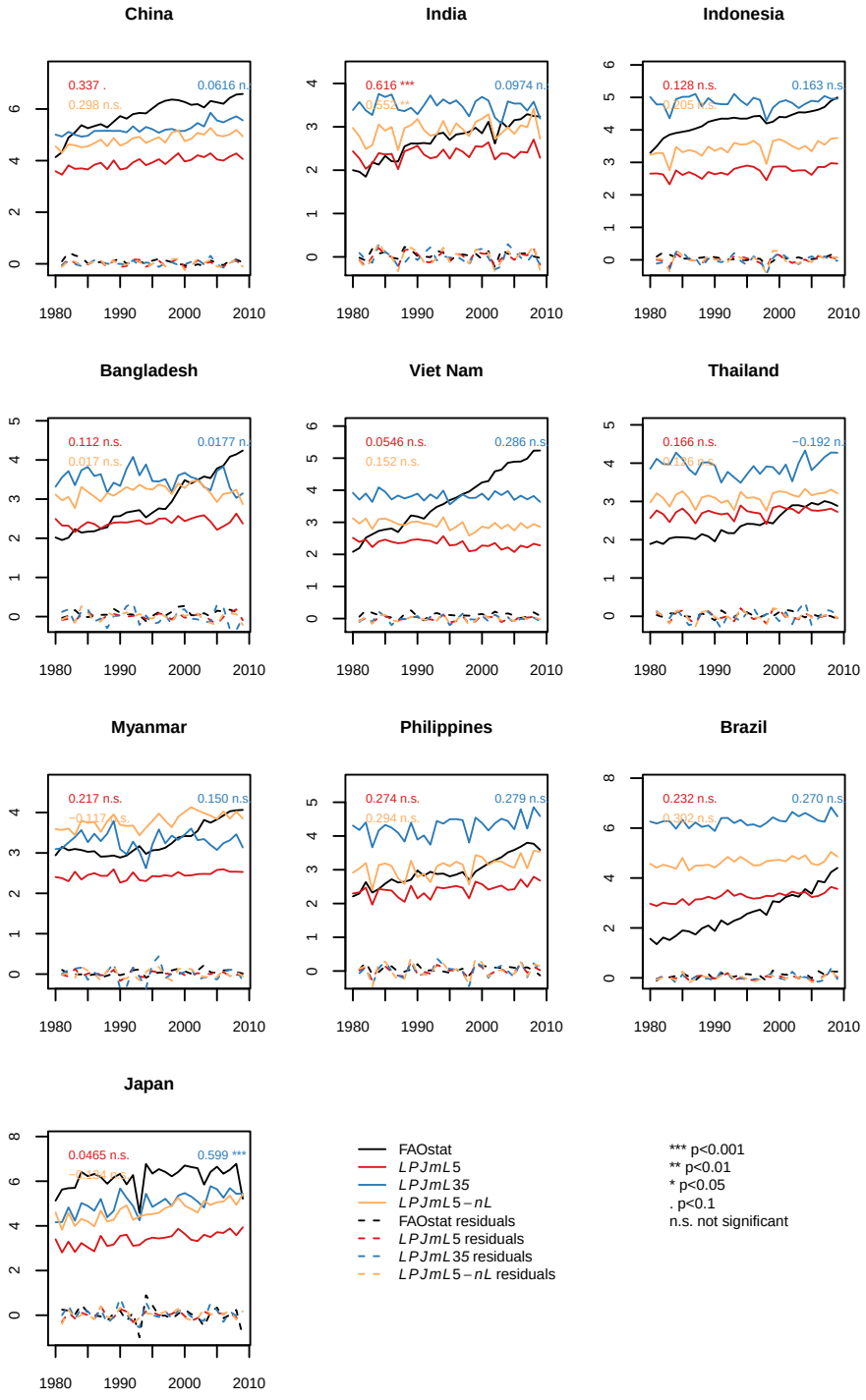

Figure S26. Rice yield simulations (in t fresh matter (FM) ha^{-1}) for the 10 top-producing countries for the carbon-only LPJmL3.5 version (*LPJmL35*), the version with N limitation (*LPJmL5*)and with unlimited N supply (*LPJmL5-nL*). The residuals plotted are the detrended observed and simulated yields.

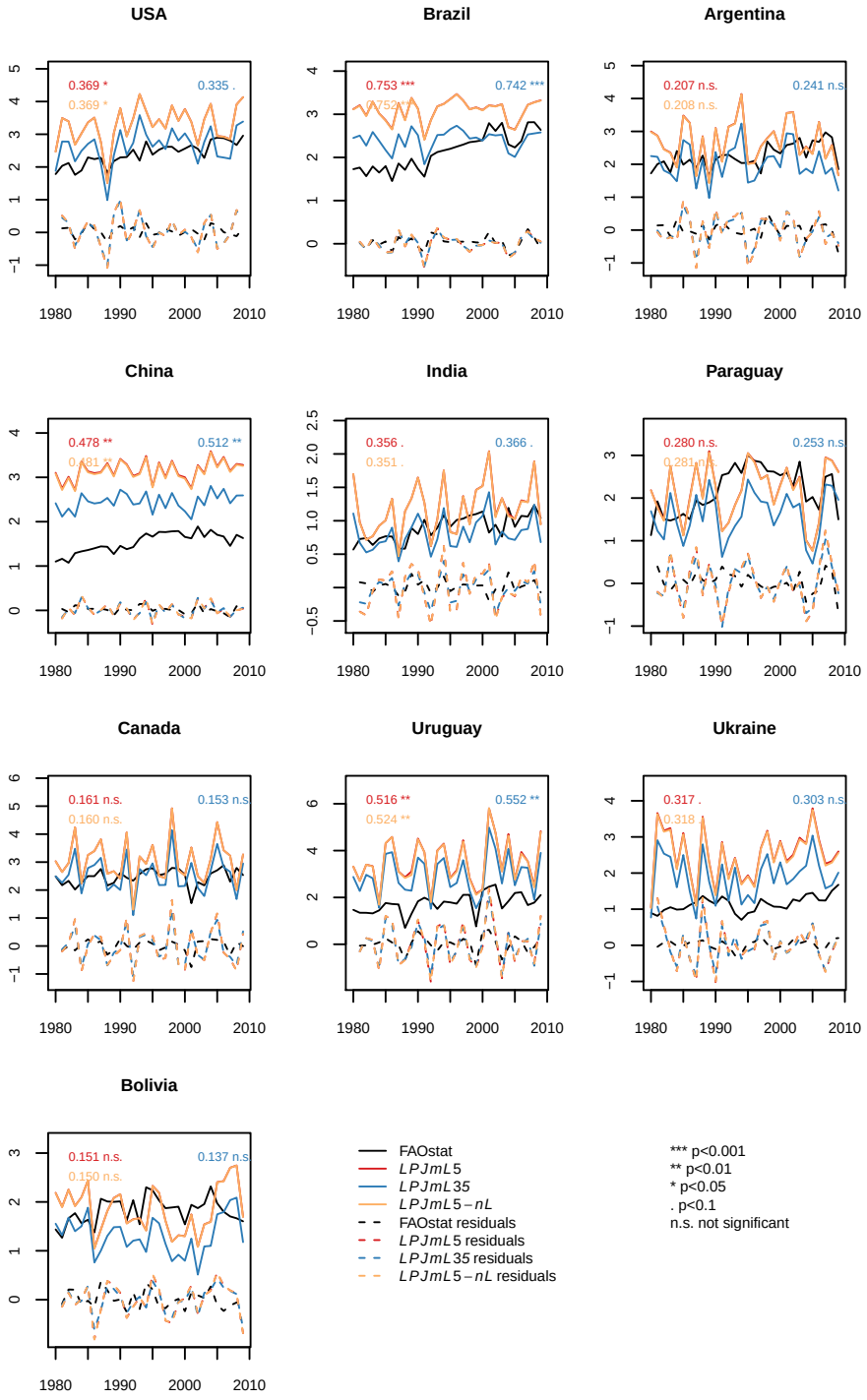

Figure S27. Soybean yield simulations (in t fresh matter (FM) ha^{-1}) for the 10 top-producing countries for the carbon-only LPJmL3.5 version (*LPJmL35*), the version with N limitation (*LPJmL5*)and with unlimited N supply (*LPJmL5-nL*). The residuals plotted are the detrended observed and simulated yields.